Characterisation of fatigue damage in a thick adhesive joint based on changes in material damping

Khoshmanesh, Sharif; Watson, Simon J.; Zarouchas, Dimitrios

DOI
10.1088/1742-6596/1618/2/022058

Publication date
2020

Document Version
Final published version

Published in
Journal of Physics: Conference Series

Citation (APA)
Khoshmanesh, S., Watson, S. J., & Zarouchas, D. (2020). Characterisation of fatigue damage in a thick adhesive joint based on changes in material damping. *Journal of Physics: Conference Series*, *1618*(2), Article 022058. https://doi.org/10.1088/1742-6596/1618/2/022058

Characterisation of fatigue damage in a thick adhesive joint based on changes in material damping

Characterisation of fatigue damage in a thick adhesive joint based on changes in material damping

Sharif Khoshmanesh, Simon J Watson, Dimitrios Zarouchas
Faculty of Aerospace Engineering, TU Delft, Kluyverweg 1, 2629 HS Delft.
E-mail: s.khoshmanesh@tudelft.nl

Abstract. The adhesively-bonded connections in a wind turbine blade, e.g. the spar cap to shear web joins, are key elements for the structural integrity of the blade. These joins can suffer from damage at the bond-line which can propagate through the structure and compromise the operation of the blade. In this paper, we determine the damping properties of a test specimen representative of that joining a spar cap and a shear web during a period of progressive damage. In addition to the experimental damping measurement, an analytical dynamic model based on the visco-elastic properties of the material is developed to relate the damping to the loss factor. The experimental results show that when a crack is initiated in the test specimen, the damping increases by around 5-7%. This value increases with the propagation of transverse cracks in the adhesive and reaches a value of 35% when the adhesive layer experiences crack saturation and the damping reaches 45 % before failure occurs. Although a significant change in the damping is observed, there is no significant change in the natural frequency (<1%) and by association little change in the stiffness of the test specimen.

1. Introduction

For the early detection of damage in a wind turbine blade, it is important to identify what property provides the most sensitive measure of that damage. If this can be done, it can be used to establish an effective blade monitoring system which in turn results in reduction of the levelised cost of energy (LCOE) [1]. This is particularly important for offshore wind farms with low accessibility [2]. In the case of vibration-based condition monitoring, the methods proposed so far rely mostly on measuring changes in the stiffness of a structure to identify damage [3–7]. But in a complex structure like a wind turbine blade, which consists of several structural elements, such as spar caps, trailing and leading edges, *etc*, changes in stiffness may not be significant unless severe damage occurs which can compromise the operation of the wind turbine [8]. The adhesively-bonded connections, *e.g.* spar caps to shear webs and the leading/trailing edges, are key elements which contribute to the structural integrity of the blade. These parts suffer from damage at the bond-line which can propagate through the structure and compromise the structural integrity [9, 10]. One property of composite material which seems to be more effective than stiffness to detect early stage of damage and its evolution is damping.

An early experimental investigation to identify damage by measuring the damping property of a material was carried out by Modena and Zonta [11, 12]. They evaluated the use of modal damping to identify manufacturing defects or structural damage in pre-cast reinforced concrete. In a similar fashion, Kawiecki [13] showed the feasibility of measuring modal damping by using arrays of piezoelectric transducers in a study on two types of concrete blocks. It was found that damping could be a useful property to detect damage in a structure. Keye [14] also verified the concept of measuring the change

in modal damping as a suitable indicator to identify damage in carbon fibre reinforced polymer (CFRP) materials.

In this paper, we attempt to characterise fatigue damage evolution in a representative wind turbine blade shear web/spar cap adhesive joint based on changes in damping. The thick shear web-spar cap adhesive joint is a key structural element of a wind turbine blade and therefore exploring the material properties of this joint, *i.e.* damping, to detect the progress of damage is a step forward in developing a reliable condition monitoring system for the blade.

2. Methodology

2.1. Damping modelling

For a linear visco-elastic material, the constitutive equation for a simple one-dimensional stress-strain relationship at time t can be written as [17],

$$\sigma(t) = \int_{-\infty}^{t} g(t-\tau)d\epsilon(\tau) \tag{1}$$

Where $\sigma(t)$ is the stress, $\epsilon(t)$ is the strain, τ is the characteristic relaxation time and $g(t)$ is the relaxation modulus associated with the material properties. The Laplace form of Equation 1 can be written as:

$$\bar{\sigma}(s) = s\bar{G}(s)\bar{\epsilon}(s) \tag{2}$$

Where $\bar{\sigma}(s)$, $\bar{G}(s)$ and $\bar{\epsilon}(s)$ are the Fourier transformed components of $\sigma(t)$, $g(t)$ and $\epsilon(t)$ respectively. If the strain is assumed to be harmonic with constant amplitude of ϵ_0 and frequency of ω,

$$\epsilon(t) = \epsilon_0 e^{j\omega t} \tag{3}$$

Then in the Laplace transformed domain,

$$\bar{\epsilon}(s) = \epsilon_0 \delta(s - j\omega) \tag{4}$$

Using the inverse definition of the Laplace transform,

$$\sigma(t) = \int_{-\infty}^{+\infty} \bar{\sigma}(s)e^{st}ds \tag{5}$$

Substituting Equation 2 and Equation 4 into Equation 5 gives:

$$\sigma(t) = \int_{-\infty}^{+\infty} s\bar{G}(s)\epsilon_0\delta(s - j\omega)e^{st}ds \tag{6}$$

Which results in:

$$\sigma(t) = j\omega\bar{G}(\omega)\epsilon_0 e^{j\omega t} \tag{7}$$

This equation relates the stress and strain for a harmonic excitation where the term $j\omega\bar{G}(\omega)$ is the dynamic modulus and is usually expressed as:

$$j\omega\bar{G}(j\omega) = E'(\omega) + jE''(\omega) \tag{8}$$

Where E' is the storage term and E'' is the loss term. The loss tangent or loss factor which represents the damping is defined as:

$$\tan(\delta(\omega)) = \frac{E''(\omega)}{E'(\omega)} \tag{9}$$

In the same way, the time domain equation of motion of a linear visco-elastic material for a single element in finite element form can be written as [16]:

$$M^{\mathrm{e}}\ddot{\mathbf{y}}(t) + g(t)K^{\mathrm{e}}\mathbf{y}(0) + \int_0^t g(t-\tau)K^{\mathrm{e}}\frac{d\mathbf{y}(\tau)}{d\tau}d\tau = \mathbf{f}(t) \tag{10}$$

where M^{e}, K^{e}, $\mathbf{y(t)}$ and $\mathbf{f}(t)$ are the mass matrix, stiffness matrix, displacement vector and force vector for a single element, respectively.

For a harmonic load, $\mathbf{f}(t) = \bar{F}(\omega)e^{j\omega t}$, the response is also harmonic, *i.e.* $\mathbf{y}(t) = \bar{Y}(\omega)e^{j\omega t}$, and Equation 10 becomes:

$$-\omega^2 M^{\mathrm{e}}\bar{Y}(\omega) + (E'(\omega) + jE''(\omega))K^{\mathrm{e}}\bar{Y}(\omega) = \bar{F}(\omega) \tag{11}$$

Where $\bar{F}(\omega)$ and $\bar{Y}(\omega)$ are the amplitude of the harmonic load and the displacement, respectively.

Equation 11 can be applied to all elements of a structure and the dynamic response of a structure to a harmonic force can be obtained. The form of the equation for the dynamic response of the whole structure is the same as that for a single element (Equation 11) except that element terms such as M^{e}, K^{e} and $\bar{Y}(\omega)$ should be replaced with M, K and Y for the whole structure. In this case, the Frequency Response Function (FRF) for the whole structure is defined as:

$$FRF = (-\omega^2 M + (E'(\omega) + jE''(\omega))K)^{-1} \tag{12}$$

where M and K are now the global mass and stiffness matrices.

From Equation 12, the analytical response of a structure in the frequency domain can be calculated. In this paper, the GHM (Golla-Hughes-McTavish) parametric form of the dynamic modulus has been used, [16]:

$$E'(\omega) + jE''(\omega) = G^0[1 + \alpha\frac{(s^2 + 2\zeta\bar{\omega}s)}{(s^2 + 2\zeta\bar{\omega}s + \bar{\omega}^2)}] \tag{13}$$

Where $s = j\omega$ and G^0, α, ζ and $\bar{\omega}$ are model parameters.

The damping can be estimated by using the experimental FRF as follows:

(i) Guess an initial values for the GHM parameters of the dynamic modulus of elasticity;
(ii) Calculate the analytical frequency response of the coupon using Equation 12;
(iii) Construct an objective function based on the squared error between the analytical and experimental values of the FRF;
(iv) Change the parameters of the GHM dynamic modulus until the objection function has been minimised;
(v) Calculate the damping from the storage and loss parts of the dynamic modulus using Equation 9.

2.2. Overview of a Blade Structure

A wind turbine blade consists of aerodynamic shells (the pressure side and suction side) and shear webs which are moulded separately and then bonded together in an assembly process using a structural adhesive. The load carrying parts of the shells (spar caps) are constructed from uni-directional composite laminates such as thick GFRM (glass fibre-reinforced materials). Shear webs are built from multi-axial fibre lay-ups and a core of balsa wood or polyvinyl chloride (PVC) foam. The web body is produced by infusion of a balsa/foam core with thin skin laminates, whereas the web foot is primarily made of multi-axial direction glass fibres. The web adhesive joint is manufactured by bonding the web foot onto the spar cap of the blade as shown in Figure 1. This web adhesive joint is a key element for the structural

integrity of the blade. If the joint suffers fatigue damage at the bond-line then this can propagate through the spar cap and lead to de-lamination and de-bonding of the spar cap from the webs.

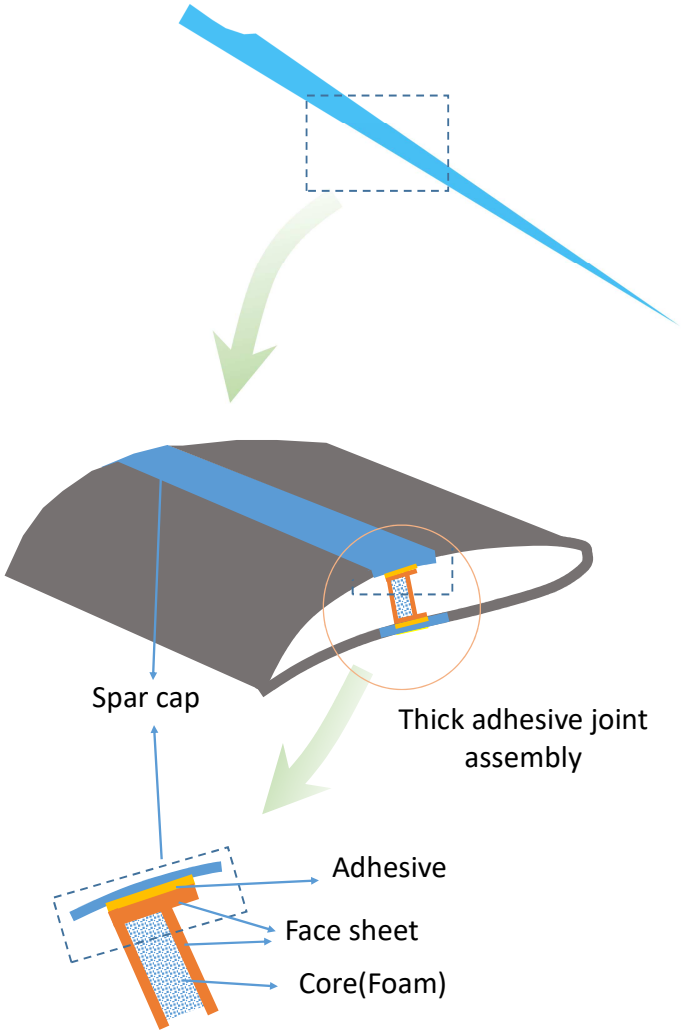

Figure 1. Schematic illustration of a spa cap/shear web thick adhesive joint

2.3. Experimental set up

In this work, we used a test specimen representative of the web adhesive joint between a shear web and spar cap subjected to fatigue tension test to study progressive damage. The testing methodology was justified following previous work using an asymmetric three-point bending fatigue test of a Henkel beam, representative of a spar to shear web assembly of a wind turbine blade, which indicated that damage progresses on the upper spar face of the beam which is under tension [10]. This test showed that damage began with transverse cracks in the bond-line of the upper spar to shear web of the beam and when the cracks reached the saturation state, damage progressed to de-bonding and final failure of the beam. In the lower spar face of the beam, no damage was observed until instability occurred in the final stage of failure. Moreover, the effect of shear stress on the fatigue performance of the beam was also relatively low. This suggested that a simple fatigue tension test can provide a realistic assessment of incipient damage in a web adhesive joint present in a wind turbine blade. The use of a simple small coupon to represent the joint

had the advantage that manufacturing flaws could be minimised ensuring that results were consistent and accurate. To represent damage in this web adhesive joint, two thick unidirectional fibre glass laminates were bonded together by adhesive and subjected to a tension fatigue test with the stress ratio (R) equal to 0.1, amplitude $0.40\sigma_u$ (where σ_u is the ultimate strength of the test specimen) and frequency 3 Hz. After 32000 cycles, the fatigue test was halted and a vibration test was carried out on the test specimen. The test set-up is shown in Figure 2. An automated hammer was used to excite the specimen and its dynamic response was measured using a laser vibrometer connected to a data acquisition system. The purpose of this modal test was to determine the experimental FRF of the test specimen. In conjunction with an analytical form of the FRF, as described in Section 2.1, it was then possible to determine the damping properties of the coupon.

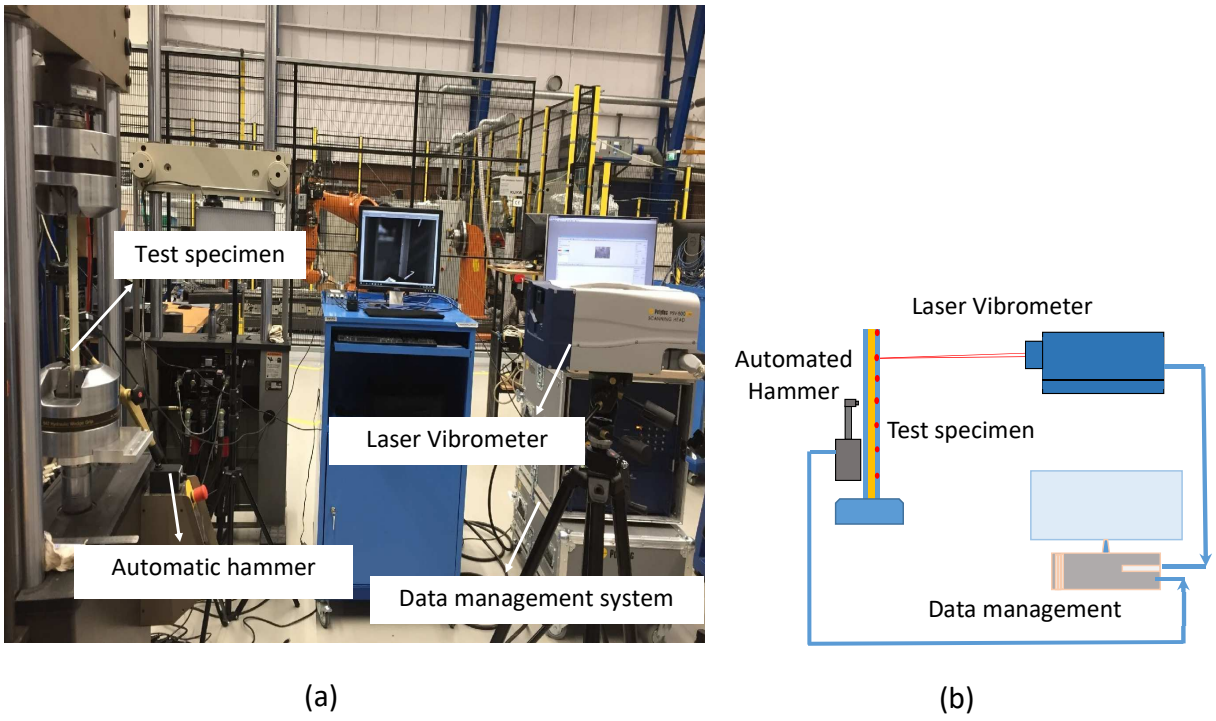

Figure 2. Experimental test set up to carry out the fatigue and modal test

Table 1. Mechanical properties and dimension of test specimen where: E_Y=Young's Modulus, σ_u=ultimate strength and ρ=volume density

	Material specification		E_Y (GPa)	σ_u (MPa)	ρ (g/cm^3)
Adhesive	Resin	Epoxy Epikote Resin MGS BPR135G2	5.5	75	1.1-1.2
	Curing agent	Epoxy Epikure Curing Agent MGS BPH1355G			
Adherent	Resin	Epoxy Epikote Resin MGS RIMR135	22.8	376	1.3-1.17
	Curing agent	Epoxy Epikure Curing Agent MGS RIMH 137			0.99
	UD fibre glass	Fibre glass cloth UD (0), 1210g/m^2, S14EU960			-

The test specimen consisted of two skins of unidirectional fibre glass which were made by the infusion of epoxy resin into three layers of unidirectional (UD(0)) fibres. These two skins were then bonded together by a layer of adhesive. The material properties of the test specimen are given in Table 1 and a schematic illustration of the test specimen is shown in Figure 3.

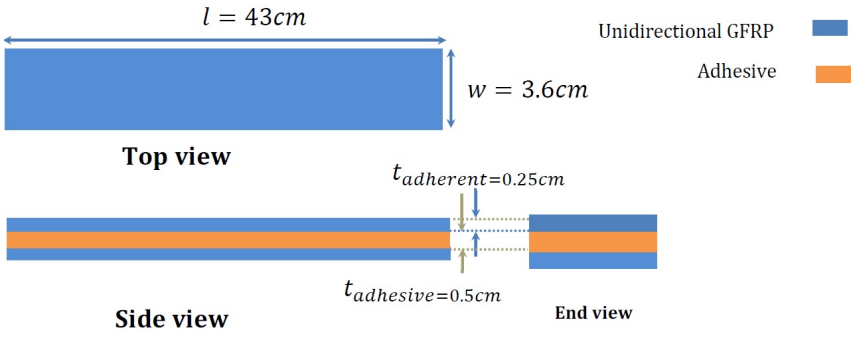

Figure 3. Schematic illustration of the test specimen

3. Results

In this section, we first present the damage propagation observed during the fatigue test. Then we determine the damping directly from the measurement data. Finally, this damping is related to the loss factor for the test specimen.

3.1. Damage evolution in the adhesive joint

After the adhesive joint was subjected to 3.1×10^4cycles during the tension fatigue test, the first signs of transverse cracks in the adhesive joint appeared.

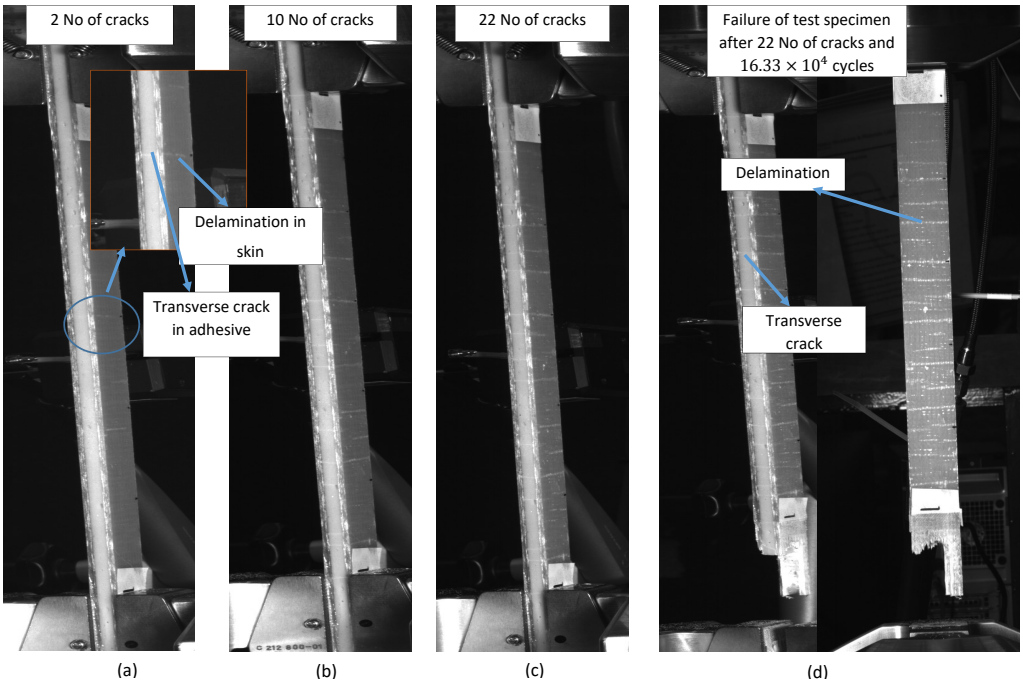

Figure 4. Damage progression in the test specimen during the tension fatigue test

As cracks occurred in the adhesive, de-lamination appeared simultaneously in the vicinity of each crack. As the depth of the cracks through the adhesive increased, so did the area of de-lamination, see Figure 4(a) and (b). This trend continued until the cracks reached the saturation phase (Figure 4(c)). Further fatigue load cycles increased the crack depth and de-lamination area and eventually led to the failure of the test specimen (Figure 4(d)).

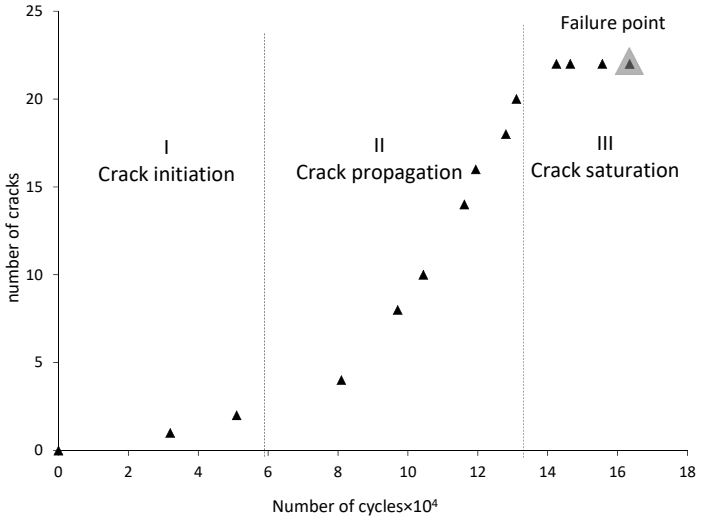

Figure 5. Increase in crack number in the test specimen during the fatigue test

In Figure 5, the number of cracks versus fatigue cycle is shown. In the initiation phase (region I), the rate of appearance of cracks was low but it increased after a certain number of fatigue cycles (region II). Eventually, the number of cracks stopped increasing (region III) but the cracks grew through the adhesive layer of the test specimen and de-lamination got progressively larger until failure occurred.

3.2. Direct measurement of damping

From the vibration test data measured using the laser vibrometer, the frequency response of the test specimen was determined at different points during the tension fatigue test. The frequency response of the test specimen in the vicinity of the 1^{st} and 2^{nd} modes of vibration are shown in Figure 6. It can be seen that the first mode of vibration showed almost no change in natural frequency as the level of damage increased. In the case of the second mode, a change could be seen between the 8-crack and the 14-crack damage cases, but after the latter degree of damage was observed, there was no further significant change in this natural frequency.

The damping was determined from the resonant response amplitude factor [16],

$$\eta = \frac{1}{A} \tag{14}$$

Where η is the damping factor and $A = \frac{W_r}{W_s}$ is the ratio of displacement at resonant frequency to static displacement (displacement in the limit that the excitation frequency $f \rightarrow 0$). The change in damping ratio as a function of the crack density is shown in Figure 7.

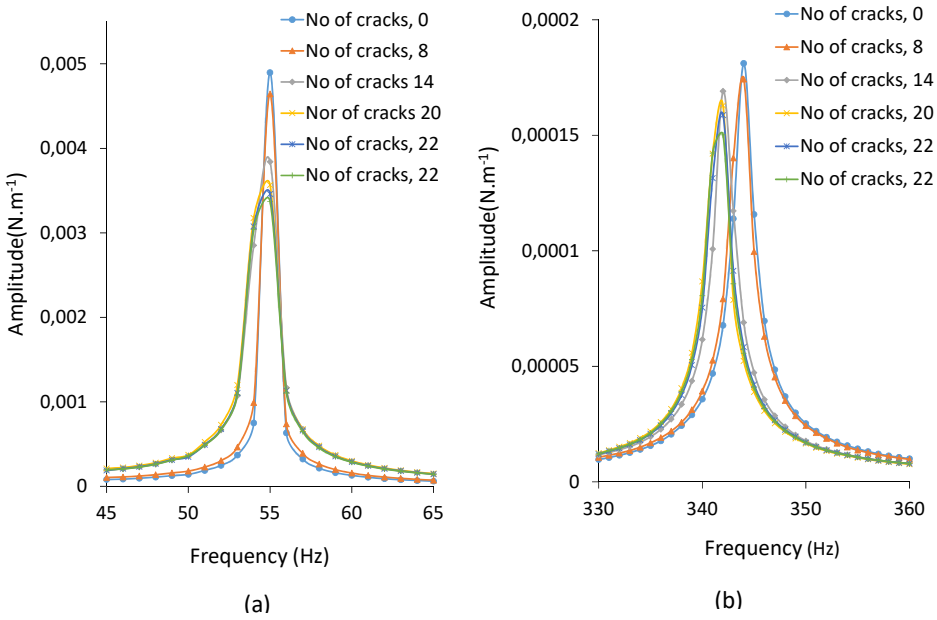

Figure 6. 1^{st} and 2^{nd} modes of vibration for five different damage cases

It can be seen that the damping ratio increased as the crack density increased but the rate of increase was lower in the initiation region than the propagation region. The cumulative change in the damping ratio in the crack initiation, crack propagation and crack saturation regions was about 7%, 35% and 45%, respectively.

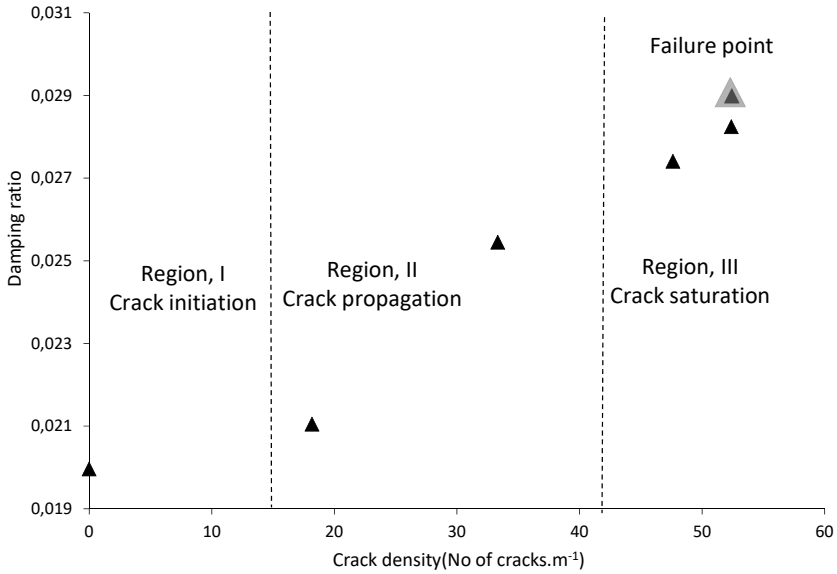

Figure 7. Damping ratio as a function of crack density

3.3. Damping and loss factor

To relate the damping to properties of the composite material, the loss factor was calculated using the method as described in Section 2.1.

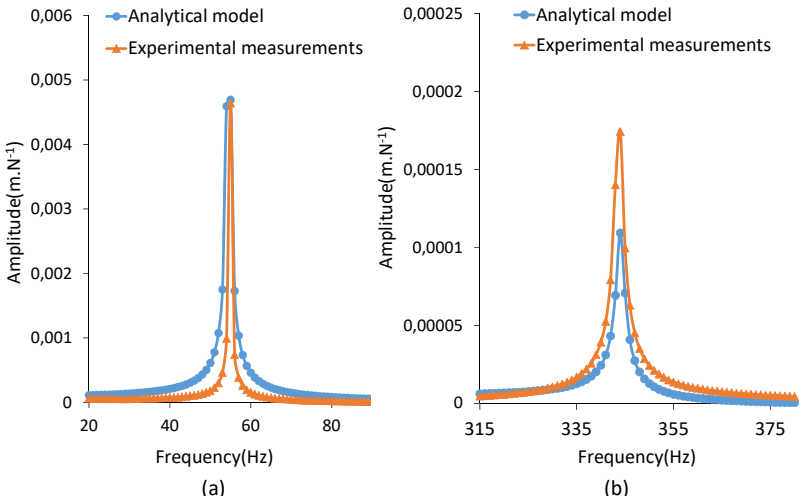

Figure 8. Comparison of the analytical and experimental frequency response function around the (a) 1^{st} and (b) 2^{nd} modes of vibration for the intact test test specimen.

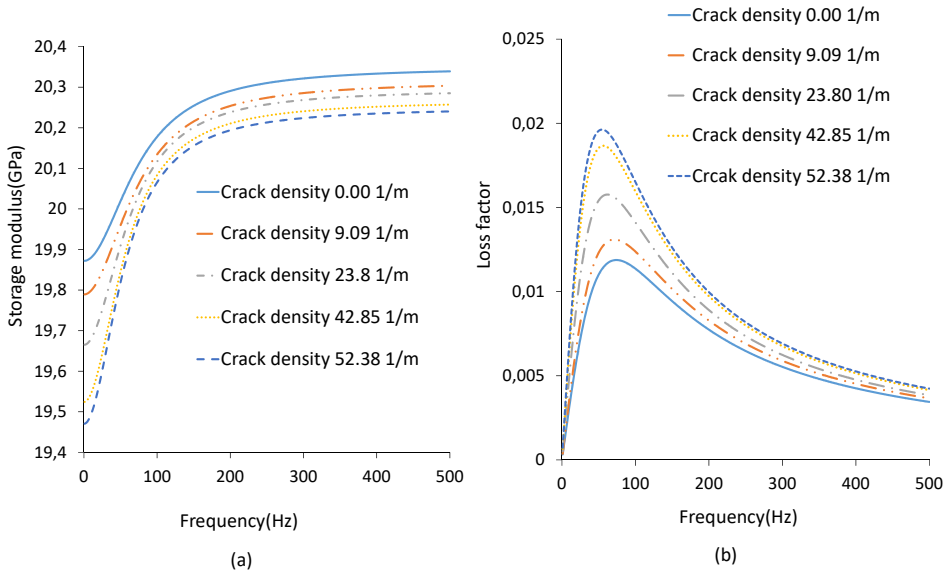

Figure 9. Storage modulus and loss factor from crack initiation until crack saturation.

The best fit of the GHM parameters of the dynamic modulus was calculated from the analytical model and thus the dynamic response of the test specimen was determined. A comparison between of the first and second mode natural frequencies determined from the analytical modelling and the experimental measurements for the intact specimen is shown in Figure 8. It can be seen that there is a reasonable match in natural frequency for both cases though some slight differences in magnitude and width. Knowing the parameters of the dynamic modulus, it is possible to determine the storage modulus, loss modulus and loss factors. The storage modulus and loss factor from initiation of cracks until the saturation phase are shown in Figures 9(a) and (b), respectively. In contrast to the changes seen in the second mode natural frequency seen in Figure 6, it can be seen here that significant progressive changes are apparent particularly in the loss factor during the entire test period.

4. Conclusion

It has been shown from the fatigue testing of a test specimen representative of an adhesive joint between a spar cap and shear web, that the first and second mode natural frequencies of the specimen are relatively insensitive to even a large degree of damage. Indeed, it was seen that the natural frequency of the second mode of vibration in the greatest damage case before failure changed by less than 1%. As stiffness is directly related to the natural frequency then by implication material stiffness shows little change with damage. By contrast, it was seen from the experimental results and through the use of an analytical model that the material damping properties of the test specimen changed substantially with increasing levels of damage. It can be concluded that the analysis of the damping properties of a wind turbine blade structure to characterise damage is more effective than trying to detect changes in material stiffness.

5. Future work

This experimental study links the loss factor of the dynamic modulus of an adhesive joint to varying levels of damage. Relating changes in the loss factor to specific areas of a wind turbine blade is not possible but connecting the loss factor to dynamic properties of the blade, e.g. the phase of a mode shape, is possible. This could be achieved by developing an analytical damage model of the blade. This is the subject of

ongoing work. Changes in the phase of nodal components of mode shapes in an area affected by damage can be directly related to changes in the material damping in that area. Although the estimation of the phase of the mode shapes of a blade structure by operational modal analysis during the operation of blade is challenging, future developments in this field such make this a possibility.

References

[1] Wenxian Y, Tavner P, Crabtree C, Feng Y, Qiu Y, 2014, *Wind Energy* **17(5)**, 673
[2] Hu B, Stumpf P, van der Deijl W, 2019, Offshore wind access 2019 TNO, R10633, Third edition.
[3] Carden P, Fanning P, 2004,*Structural Health Monitoring* **3(4)**, 355
[4] Montalvao D, Maia M, Ribeiro R, 2006,*Shock and Vibration Digest* **38(4)**, 295
[5] Xuan K, Chun-Sheng C, Jiexuan H, 2017, The state of the art on framework of vibration based structural damage identification for decision making,*Applied Sciences*, **7(5)**, 1.
[6] Hoon S, Charles R, Farrar R, Francois H, Devin S, Daniel W, Stinemates R, Jerry C, A review of structural health monitoring literature: 1996–2001 (LA-13976-MS).
[7] Doebling W, Farrar PM, 1998, *The Shock and Vibration Digest* **30**, 91.
[8] Al-Khudairi O, Hadavinia H, Little C, Gillmore G, Greaves P, Dyer K, 2017,*Materials* **10(10)**, 1.
[9] Zarouchas D, Makris A, Sayer F, van Hemelrijck D, van Wingerde A, 2012, *Composites Part B: Engineering* **43(2)**, 647
[10] Sayer F, Antonion A, van Wingerde A, 2012, *Adhesion and Adhesives* **37(1)**, 129
[11] Modena C, Sonda D, Zonta D, Damage localization in reinforced concrete structures by using damping measurements, 1999 Proceedings of the International Conference on Damage Assessment of Structures(DAMAS 99), Dublin University, Dublin, Ireland, June 28–30, trans Tech Publications Ltd,.
[12] Zonta D, Modena C, Bursi S, Analysis of dispersive phenomena in damaged structures, 2000, Proceedings of European COST F3 Conference on System Identification and Structural Health Monitoring, Madrid University, Madrid, Spain, June,ISBN: 9788486189686.
[13] Kawiecki G, 2001, *Smart Materials and Structures* **10(3)**, 466
[14] Keye S, Rose M, Sachau D, Localizing delamination damages in aircraft panels from modal damping parameters, 2001, Proceedings of the 19^{th} international modal analysis conference (IMAC XIX), Society for Experimental Mechanics, Florida, USA, February 5-8.
[15] Nashif A, Jones D and Henderson J, Vibration Damping, 1985 Wiley-Interscience, Corporate Headquarters 111 River Street, Hoboken, NJ 07030-5774-USA, ISBN 978-0471867722.
[16] McTavish J and Hughes C, 1993,*Vibration and Acoustics* **11**, 103
[17] Lakes R, Viscoelastic materials, 2009, Cambridge University Press, 32 Avenue of the Americas, New York, NY 10013-273-USA, ISBN 978-0521885683.